Linear-Quadratic Regulator Controller with Fuzzy based High Performance Frequency Converter Controlled Variable-Speed Wind Generator

[1]M.Shobha, [2]B.Naredra

[1,2]*Assistant Professor*

Department Of EEE

CVRT Engineering college, Tadipatri

Abstract—This paper proposes an optimal control strategy with a view to achieving the best performance of a wind energy conversion system (WECS) with fuzzy logic. The optimal control strategy depends on the linear-quadratic regulator (LQR) algorithm with fuzzy logic, which provides fast convergence and less mathematical intricacy and harmonic control. The machine- and the grid-side converter/inverter are adjusted using the LQR controller. In this study, the system model and its control strategies are illustrated. Wind speed data are considered in this study for achieving realistic responses. The system performance is evaluated by comparing the results obtained using the LQR controller with that realized when the grey wolf optimizer algorithm-based optimized proportional-integral controllers and fuzzy logic controller are used, taken into account severe network disturbances. The simulation studies are extensively performed through the MATLAB/Simulink environment that prove the validity of the LQR controller for improving the performance of the WECS with harmonic controlling. The simulation results are compared with the experimental results for more validation.

Index Terms—Frequency converter, linear-quadratic regulator (LQR), permanent-magnet synchronous generator, power system control, variable-speed wind turbine.

I.INTRODUCTION

Wind power is considered the mainstream clean energy source in the electric power generation. Political matters, the depletion in fossil-fuel, and the rise in fuel prices are the main reasons that allow wind power to penetrate the power networks. In 2017, the cumulative global wind power capacity reached 539 GW, which is an increase of 11% compared with 2016 [1]. By 2022, it is predictable that the cumulative wind power capacity shall realize 840 GW worldwide [1]. The variable-speed wind turbine generator systems (WTGSs) are vastly applied in wind power applications because of the lower mechanical stress, the better control capability, and the high efficiency that they present than the fixed-speed [2], [3]. Different classes of electric machines are utilized in the variable-speed WTGSs. Among them, permanent-magnet synchronous generator (PMSG) has received great concerns in the modern wind industry because of the self-excitation and the high efficiency [4]–[6].

The variable-speed (VS)-WTGS driving PMSG is integrated into the grid via a full capacity frequency converter. The frequency converter consists of two power converters, which are tied through a dc-link [3], [6]. Each converter has six insulated gate bipolar transistors (IGBTs). However, this topology uses more controlled switches, resulting in the system is more expensive and less reliable. Few research efforts have been exerted to produce high-performance, simple, and reliable power converters with reduced number of power switches, losses, and cost in order to track the industrial requirements. The four-switch three-phase (FSTP) converter has been presented with four power switches as a substitute to the six-switch three-phase (SSTP) converter. The FSTP converter has some features over the SSTP converter, such as reduced the number of utilized switches by one-third, reduced the complexity of the driving circuits, where there are only two controlled branches which require only two interface driving circuits, and the maximum common mode voltage of the FSTP converter is two-thirds that of SSTP converter [7], [8].

Traditionally, the control of the machine-side converter (MSC) and the grid-side inverter (GSI) uses the proportional-integral (PI) controllers because of the robustness and the wide stability margins of these controllers [3]. However, these controllers have high

sensitivity to the system nonlinearity and variables' uncertainty. Several optimization approaches are presented for optimally designing the PI controllers [9]–[15]. Shuffled frog leaping algorithm [10], harmony search algorithm [11], grey wolf optimization [3], whale optimization algorithm [13], gravitational search algorithm [14], and water cycle algorithm [15] are proposed to design proper values of multiple PI controllers under the cascaded structure to enhance the behavior of grid-tied WECSs.

The grey wolf optimizer (GWO) algorithm is an evolutionary algorithm, which is used to optimally-tuning the PI controllers. The GWO is a new meta-heuristic optimization-based algorithm, which describes the grey wolves in wildlife [14].

The procedures of hunting behavior for the GWO algorithm are drawn by the grey wolves as; search, encircle, and attack the prey [16]–[18]. The GWO is characterized by the simple implementation, free-derivative technique, and lower operators to be adjusted compared to other optimization algorithms. To overcome the complicated control strategies, Linear-Quadratic Regulator (LQR) is an alternative controller, presented to achieve the best dynamic performance and robust control stability. Generally, LQR is a state-feedback controller that utilizes a state-space approach to design and control the system. In LQR controller, the optimization relies on the minimization of quadratic cost function [19]. The main merits of LQR controller include superior performance without sophisticated algorithms and extra computational analysis. The LQR controller is simple, easy to implement, and has a lower memory capacity [20]. These advantages of the LQR represent the impetus to use it in this study to obtain better results than other traditional controllers. The LQR controller has been extensively applied to efficiently control many industrial applications such as aerospace engineering and technology [21], discrete-time control systems [22], hybrid systems [23], laser beam shaping [24], electric drives [25] and wind energy systems [26], [27].

This paper introduces the LQR controller-based an optimal control scheme for improving the characteristics of a grid-connected variable-speed WTGS. A low-cost frequency converter, which consists of two identical FSTP converters, is presented. To control the MSC and the GSI, a hysteresis current controller is considered. Moreover, a rotor position estimator based on a sliding mode observer (SMO) technique is established to reduce the cost and the hardware intricacy. The main new contribution of this study is the novel application of the LQR controller to control the FSTP converters of the VS-WTGS. The proposed controller validity is verified with both the simulation and experimental results under grid disturbance conditions. The model system and its control schemes are illustrated. Realistic wind speed data are considered in this study to achieve realistic responses. The system performance is evaluated by comparing the results obtained using the proposed LQR controller with that realized when the GWO algorithm-based optimized PI controllers are used, taken into account severe network fault conditions. The simulation analyses are performed through the MATLAB/Simulink environment that verifies the validity of the LQR controller with fuzzy logic controller.

II.LITERETURE SURVEY

"Co-ordinated control strategy for hybrid wind farms with PMSG and FSIG under unbalanced grid voltage condition"

This paper investigates a control strategy for a wind farm with the direct-driven permanent-magnet synchronous generators (PMSG)-baed wind turbines and the fixed speed induction generators (FSIG)-based wind turbines under unbalanced grid voltage condition. By controlling the PMSG-based wind farm to inject negative-sequence current for decreasing voltage unbalance factor (VUF) at point of common coupling (PCC), the double grid frequency oscillations in electromagnetic torque, active, and reactive power output from the FSIG-based wind farm can be suppressed. In this paper, the maximum amplitude of the negative-sequence current provided by the PMSG-based wind farm under different average active power output and different VUF conditions is deduced, and the impacts of its phase angle on the VUF mitigation control effect are further studied. The improved control strategy of injecting negative-sequence current from the PMSG-based wind farm by the modified negative-sequence voltage and current double closed-loop control system is then developed. Finally, the correctness of theoretical analysis and the effectiveness of the

proposed control strategy are validated by the experimental results.

"Hybrid ANFIS-GA-based control scheme for performance enhancement of a grid-connected wind generator,"

This study presents a novel application of a hybrid adaptive neuro-fuzzy inference system (ANFIS)-genetic algorithm (GA)-based control scheme to enhance the performance of a variable-speed wind energy conversion system. The variable-speed wind turbine drives a permanent-magnet synchronous generator, which is connected to the power grid through a frequency converter. A cascaded ANFIS-GA controller is introduced to control both of the generator-side converter and the grid-side inverter. ANFIS is a non-linear, adaptive, and robustness controller, which integrates the merits of the artificial neural network and the FIS. A GA-based learning design procedure is proposed to identify the ANFIS parameters. Detailed modelling of the system under investigation and its control strategies are demonstrated. For achieving realistic responses, real wind speed data extracted from Zaafarana wind farm, Egypt, are considered in the analyses. The effectiveness of the ANFIS-GA controller is compared with that obtained using optimised proportional-integral controllers by the novel grey wolf optimiser algorithm taking into consideration severe grid disturbances. The validity of the ANFIS-GA control scheme is verified by the extensive simulation analyses, which are performed using MATLAB/Simulink environment. With the ANFIS-GA controller, the dynamic and transient stability of grid-connected wind generator systems can be further enhanced.

III. PHOTOVOLTAIC INVERTER

PV unit   : A PV unit consists of number of PV cells that converts the energy of light

directly into electricity (DC) using photovoltaic effect.

1. Inverter   : Inverter is used to convert DC output of PV unit to AC power.
2. Grid   : The output power of inverter is given to the nearby electrical grid for the

power generation.
3. MPPT   : In order to utilize the maximum power produced by the PV modules, the

power conversion equipment has to be equipped with a maximum power point tracker (MPPT). It is a device which tracks the voltage at where the maximum power is utilized at all times.

Photovoltaic cell and array modeling

A PV cell is a simple p-n junction diode that converts the irradiation into electricity. Fig.3.2 illustrates a simple equivalent circuit diagram of a PV cell. This model consists of a current source which represents the generated current from PV cell, a diode in parallel with the current source, a shunt resistance, and a series resistance.
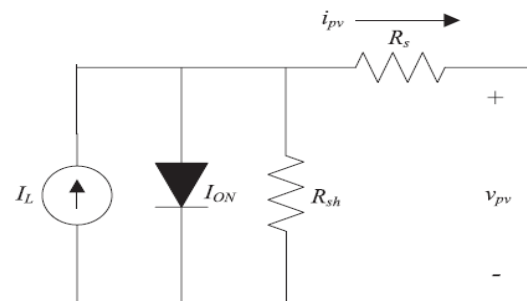

Fig.3.2 Equivalent circuit diagram of the PV cell

IV.DC-DC CONVERTERS

A DC-DC converter with a high step-up voltage, which can be used in various applications like automobile headlights, fuel cell energy conversion systems, solar-cell energy conversion systems and battery backup systems for uninterruptable power supplies.Theoritically, a dc-dc boost converter can attain a high step-up voltage with a high effective duty ratio.But,in practical, the step-up voltage gain is restricted by the effect of power switches and the equivalent series resistance(ESR) of inductors and capacitors.Generally a conventional boost converter is used to get a high-step-up voltage gain with a large duty ratio. But, the efficiency and the voltage gain are restricted due to the losses of power switches and diodes, the equivalent series resistance of inductors and capacitors and the reverse recovery problem of diodes. Due to the leakage inductance of the transformer, high voltage stress and power dissipation effected by the active switch of these converters. To reduce the Voltage spike, a resistor-capacitor –diode snubbed can be employed to limit the voltage stress on the

active switch. But, these results in reduction of effiency.Based on the coupled inductor; converters with low input ripple current are developed. The low input current ripple of these converters is realized by using an additional LC circuit with a coupled inductor.

V.WIND POWER

Wind is abundant almost in any part of the world. Its existence in nature caused by uneven heating on the surface of the earth as well as the earth's rotation means that the wind resources will always be available. The conventional ways of generating electricity using non renewable resources such as coal, natural gas, oil and so on, have great impacts on the environment as it contributes vast quantities of carbon dioxide to the earth's atmosphere which in   turn will cause the temperature of the earth's surface to increase, known as the green house effect. Hence, with the advances in science and technology, ways of generating electricity using renewable energy resources such as the wind are developed. Nowadays, the cost of wind power that is connected to the grid is as cheap as the cost of generating electricity using coal and oil. Thus, the increasing popularity of green electricity means the demand of electricity produced by using non renewable energy is also increased accordingly.
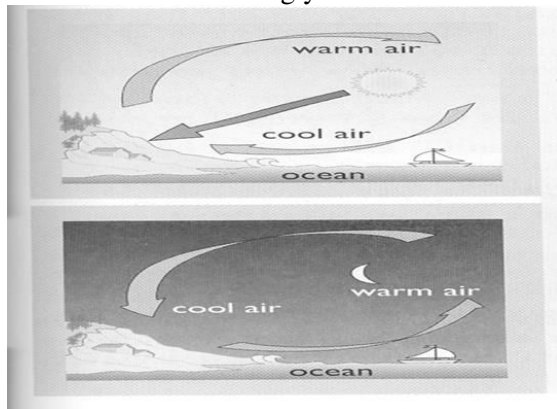

Fig: Formation of wind due to differential heating of land and sea

VI.Introduction to fuzzy

In recent years, the number and variety of applications of fuzzy logic have increased significantly. The applications range from consumer products such as cameras, camcorders, washing machines, and microwave ovens to industrial process control, medical instrumentation, decision support systems, and portfolio selection. To understand why use of fuzzy logic has grown, you must first understand what is meant by fuzzy logic.

Fuzzy logic has two different meanings. In a narrow sense, fuzzy logic is a logical system, which is an extension of multivalve logic. However, in a wider sense fuzzy logic (FL) is almost synonymous with the theory of fuzzy sets, a theory which relates to classes of objects with un sharp boundaries in which membership is a matter of degree. In this perspective, fuzzy logic in its narrow sense is a branch of FL. Even in its more narrow definition, fuzzy logic differs both in concept and substance from traditional multivalve logical systems.

In fuzzy Logic Toolbox software, fuzzy logic should be interpreted as FL, that is, fuzzy logic in its wide sense. The basic ideas underlying FL are explained very clearly and insightfully in Foundations of Fuzzy Logic. What might be added is that the basic concept underlying FL is that of a linguistic variable, that is, a variable whose values are words rather than numbers. In effect, much of FL may be viewed as a methodology for computing with words rather than numbers. Although words are inherently less precise than numbers, their use is closer to human intuition. Furthermore, computing with words exploits the tolerance for imprecision and thereby lowers the cost of solution.

Another basic concept in FL, which plays a central role in most of its applications, is that of a fuzzy if then rule or, simply, fuzzy rule. Although rule based systems have a long history of use in Artificial Intelligence (AI), what is missing in such systems is a mechanism for dealing with fuzzy consequents and fuzzy antecedents. In fuzzy logic, this mechanism is provided by the calculus of fuzzy rules. The calculus of fuzzy rules serves as a basis for what might be called the Fuzzy Dependency and Command Language (FDCL). Although FDCL is not used explicitly in the toolbox, it is effectively one of its principal constituents. In most of the applications of fuzzy logic, a fuzzy logic solution is, in reality, a translation of a human solution into FDCL.

A trend that is growing in visibility relates to the use of fuzzy logic in combination with neuro computing and genetic algorithms. More generally, fuzzy logic, neuron computing, and genetic algorithms may be viewed as the principal constituents of what might be called soft computing. Unlike the traditional, hard computing, soft computing accommodates the imprecision of the real world.

The guiding principle of soft computing is: Exploit the tolerance for imprecision, uncertainty, and partial truth to achieve tractability, robustness, and low solution cost. In the future, soft computing could play an increasingly important role in the conception and design of systems who's MIQ (Machine IQ) is much higher than that of systems designed by conventional methods.

Among various combinations of methodologies in soft computing, the one that has highest visibility at this juncture is that of fuzzy logic and neuron computing, leading to neuron fuzzy systems. Within fuzzy logic, such systems play a particularly important role in the induction of rules from observations. An effective method developed by Dr. Roger Jang for this purpose is called ANFIS (Adaptive Neuron Fuzzy Inference System). This method is an important component of the toolbox.

The fuzzy logic toolbox is highly impressive in all respects. It makes fuzzy logic an effective tool for the conception and design of intelligent systems. The fuzzy logic toolbox is easy to master and convenient to use. And last, but not least important, it provides a reader friendly and up to date introduction to methodology of fuzzy logic and its wide ranging applications.
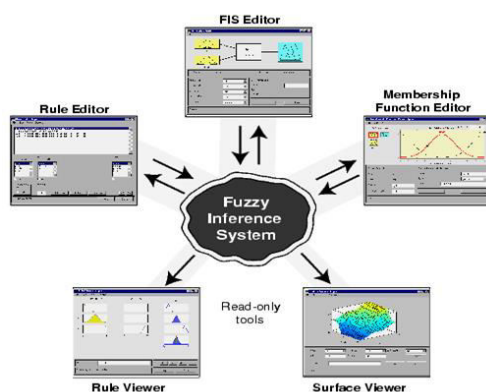

Fig. The primary GUI tools of the fuzzy logic toolbox

VI. PROPOSED SYSTEM AND CONTROL DESIGN
MODEL OF THE WIND TURBINE

The output power extracted from the wind is mathematically described as [28]-[30]:

$$P_\omega = 0.5\rho\pi R^2 V_\omega^3 C_P(\lambda, \beta) \tag{1}$$

where P_ω represents the output power from the wind [W], ρ denotes the density of air [kg/m3], R represents the radius of the turbine's blade [m], V_ω is the wind speed [m/s], and C_P denotes the power coefficient, λ represents tip speed ratio, and β denotes blade pitch angle [deg.].
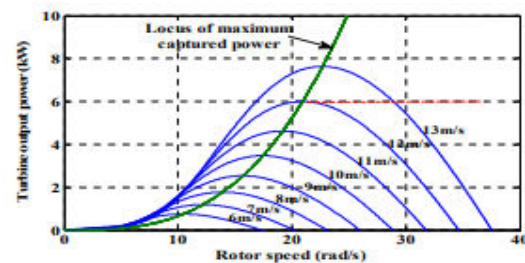

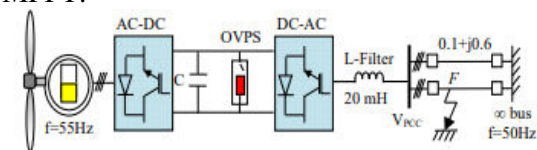**Fig. 1.** Wind turbine characteristics with MPPT.

Fig. 2. Model system.

The C_P coefficient can be described as follows [3]:

$$C_P(\lambda, \beta) = 0.5(\lambda - 0.022\beta^2 - 5.6)e^{-0.17\lambda} \tag{2}$$

$$\lambda = \frac{\omega_T R}{V_w} \tag{3}$$

where ω_T denotes the blade rotor speed [rad/s]. Fig. 1 points out the characteristics of the wind turbine with the maximum power point tracking (MPPT). The maximum output power captured from the wind in terms of rotor speed is described by the following [6]:

$$P_{max} = 0.5\rho\pi R^2 \left(\frac{\omega_T R}{\lambda_{opt}}\right)^3 C_{P-opt} \tag{4}$$

where C_{P-opt} and λ_{opt} are the optimum values of the C_P and λ, respectively.

MODEL SYSTEM

Fig. 2 shows the system modelling to explain the efficacy of the proposed LQR controller utilized for adjusting the frequency converter of the variable-speed wind turbine (VSWT) driving PMSG. The VSWT-PMSG system

consists of a VSWT, a PMSG connected to the electric network via a full capacity frequency converter, and a double-circuit transmission line. In this study, the rated power and frequency of the PMSG is 6.0 kW and 55 Hz, respectively. More details of the PMSG data are reported in [28].

SPEED ESTIMATOR BASED ON SMO TECHNIQUE

The information of the rotor position signal of the PMSG is necessary needed for the system control. In this study, the sliding-mode observer (SMO) technique is applied for sensorless rotor position estimation of the PMSG. The observer depends on the measured stator voltages and currents of the PMSG, where the $\alpha\beta$ coordinates of the actual voltages and currents are the inputs to the SMO. The $\alpha\beta$ stator current components are given as [31]:

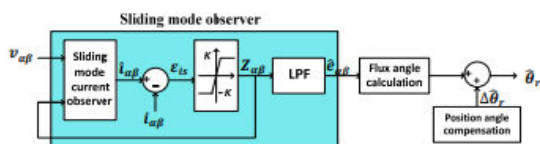$$\frac{di_\alpha}{dt} = -\frac{R_s}{L_s}i_\alpha + \frac{1}{L_s}v_\alpha - \frac{1}{L_s}e_\alpha$$

Fig. 3. Schematic diagram of the rotor position estimation using SMO.

$$\frac{di_\beta}{dt} = -\frac{R_s}{L_s}i_\beta + \frac{1}{L_s}v_\beta - \frac{1}{L_s}e_\beta$$

$$e_\alpha = -\omega_e \lambda_m \sin\theta_r$$

$$e_\beta = \omega_e \lambda_m \cos\theta_r$$

where $R0$ is stator resistance of the PMSG, $L0$ is the synchronous inductance of the PMSG, PMSG, (v_α, v_β), (i_α, i_β), and (e_α, e_β) are the $\alpha\beta$ quantities of the stator voltages, currents, and back EMFs, respectively; and $\theta_\Box$ represents the rotor position. The estimated $\alpha\beta$ stator current components using SMO technique can be expressed as:

$$\frac{di_\alpha}{dt} = -\frac{R_s}{L_s}\hat{i}_\alpha + \frac{1}{L_s}v_\alpha - \frac{1}{L_s}\hat{e}_\alpha$$

$$\frac{di_\beta}{dt} = -\frac{R_s}{L_s}\hat{i}_\beta + \frac{1}{L_s}v_\beta - \frac{1}{L_s}\hat{e}_\beta$$

$$Z_{\alpha\beta} = k \, sgn \, \varepsilon_{is} = k \, sgn \, (\hat{i}_{\alpha\beta} - i_{\alpha\beta})$$

where superscript ^ denotes the estimated quantities; $Z_{\alpha\beta}$ is the switching signal; sgn( ) represents the sign function, and k represents the switching gain of the observer. To guarantee the convergence of the SMO, k

should be selected such that $\varepsilon_{is} \cdot \left(\frac{d}{dt}\varepsilon_{is}^T\right) < 0$. Fig. 3 clarifies the schematic diagram of the SMO. A low pass filter is utilized to obtain the estimated back-EMF from the $Z_{\alpha\beta}$ as follows:

$$\hat{e}_\alpha = \frac{\omega_c}{S+\omega_c}Z_\alpha \tag{12}$$

$$\hat{e}_\beta = \frac{\omega_c}{S+\omega_c}Z_\beta \tag{13}$$

Where ω_c represents the cut-off frequency of the filter. The estimated rotor position can be obtained as:

$$\hat{\theta}_r = -tan^{-1}\left(\frac{\hat{e}_\alpha}{\hat{e}_\beta}\right) \tag{14}$$

As the filter causes phase delay, compensation is needed for the estimated angle, which is expressed as:

$$\Delta\hat{\theta}_r = tan^{-1}\left(\frac{\omega_e}{\omega_c}\right) \tag{15}$$

Hence, the estimated rotor speed can be obtained using the derivative of the estimated rotor angle.

FREQUENCY CONVERTER MODELING AND CONTROL STRATEGY

In this study, Fig. 4 presents the electrical configuration of the proposed VSWT-PMSG topology. The frequency converter of VSWT-PMSG illustrated in Fig. 4, consists of two identical FSTP power converters, one of them for the converter and the other for the inverter, and a two-split capacitor in the dc-link. A
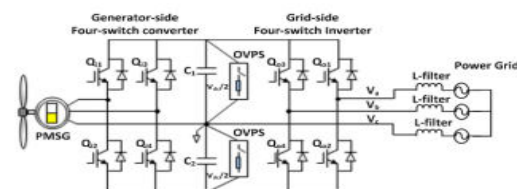

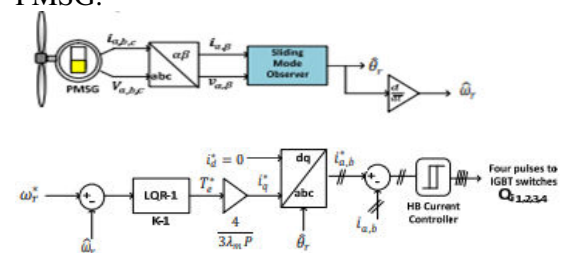
Fig. 4. Electrical configuration of VSWT-PMSG.

Fig. 5. Control blocks for the MSC.

FSTP inverter with the two-split capacitor achieves a balanced three-phase output to the power grid with adjustable voltage and frequency. The generator's terminals are directly tied to the two pulse width modulation voltages of the converter and the midpoint of the two-split capacitor. The three-phase power

grid is tied to the two-leg inverter's output and the same midpoint. The midpoint of the split-capacitor acts as the third phase for the converter/inverter.

This control scheme is simple and achieves a good dynamic response [7]. The output phase voltages of the FSTP inverter as a function of switching states, $S\square$ and $S\square$ of the power switches and the voltage across the two-split capacitor, $V\circ 6\pi\square$, are expressed in a matrix form as follows:

$$\begin{bmatrix} V_a \\ V_b \\ V_c \end{bmatrix} = \frac{v_{dc}}{3}\begin{bmatrix} 4 & -2 \\ -2 & 4 \\ -2 & -2 \end{bmatrix}\begin{bmatrix} S_a \\ S_b \end{bmatrix} + \frac{v_{dc}}{3}\begin{bmatrix} -1 \\ -1 \\ 2 \end{bmatrix} \qquad (16)$$

A. The MSC

The MSC takes responsibility for capturing the maximum output power from the wind turbine and transmitting it to the grid. To achieve this target, a hysteresis current controller is used where the estimated generator speed $(\hat{\omega}_r)$ is forced to track the reference speed (ω_r^*). The error signal between the reference and measured speeds generates the torque command (T_e^*) through the LQR controller. The q-axis current (i_q^*) is calculated from the T_e^* to control the active power. The i_d^* is chosen zero to ensure a maximum torque per minimum current. As a result, the resistive losses in the PMSG can be minimized. The dq-axes current quantities are converted to the three-phase reference currents using the estimated rotor angle (θ_r). The sensed two-phase currents $(i_{a,b})$ of the PMSG are then
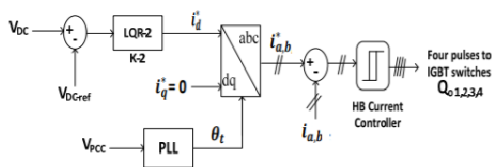

Fig. 6. Control blocks for the GSI.

compared with the two-phase reference currents $(i_{a,b}^*)$ using two hysteresis comparators. The output signals of these comparators produce the switching pulses to the four electronic switches. The block diagram for the MSC is shown in Fig. 5.

B. The GSI

The main purpose of using the GSI is to adjust the dc-link voltage (V_{DC}) and keep it constant at the desired value and perform a unity power factor operation at the grid. In this study, two dc-link capacitors with rated values of 500 μF are considered and the V_{DC} is chosen 700 V for each one. The operation of the GSI is performed using the set zero to provide unity power factor operation at the grid terminals. The dq-axes hysteresis current controller, where the V_{DC} is forced to track the dc-link reference voltage (V_{DC-ref}). The error signal between the reference and actual dc-link voltages produces the d-axis current (i_d^*) using the LQR controller. The i_q^* can control the reactive power. So, it is currents are transformed to the abc components using the transformation the voltages at the point of common coupling (V_{PCC}). The actual two-phase currents at the grid-side $(i_{a,b})$ compared with the two-phase current commands $(i_{a,b})$ using two independent hysteresis comparators that produce the firing pulses to the two-leg inverter. The block diagram of the GSI control is illustrated in Fig. 6 [32]-[34].

THE PROPOSED CONTROLLERS

A. LQR controller

The LQR is an optimal controller that employs a state-space system form to enhance the system response by using the suitable choice of state-feedback gain matrix (K). A pole placement method which depends on the desired location of poles is used to determine the values of K. Although the values of matrix (K) are easy to be calculated using this method, the LQR is a good choice for higher order and multi-input system where the best response of the closed-loop system is reached. LQR depends on the cost function in order to define the optimal pole location. It uses differential equations that illustrate the paths of the control variables to decrease the cost function. The control input (u_c) is used to realize the optimal solution in which the quadratic cost function (J) can be minimized [19].

$$J = \int_0^\infty (x_e^T Q x_e + u_c^T R u_c)\, dt \qquad (17)$$

where Q and R denote the weighted-matrices, which are

selected to make the poles at the required location. When the matrix Q has large values, the closed-loop poles $(E = A - BK)$ are becoming further left in the s-plane. As a result, the error decreases rapidly to zero. The matrix K is determined by the suitable selection of the weighted-matrices, where Q and R are positive semi-definite and positive definite, respectively. The control input selected to decrease the quadratic cost function J is achieved as:

$$u_c = -Kx_e \qquad (18)$$

where $x_e = x_{ref} - x_{actual}.$

The design of the optimal control scheme is realized by solving the Algebraic Riccati Equation:

$$A^T P + PA - PBR^{-1}B^T P + Q = 0 \qquad (19)$$

Thus, the optimal K is obtained as:

$$K = R^{-1}B^T P \qquad (20)$$

In this investigation, the control system is linearized in the state-space form as follows:

$$\dot{X} = AX + BU \qquad (21)$$
$$Y = CX \qquad (22)$$

where X refers to the state variables, U represents the control input, and Y represents the control output. For the PMSG model, the X, U, and Y can be expressed as follows:

$$X = [i_{d-PMSG} \; i_{q-PMSG} \; \omega_e]^T \qquad (23)$$
$$U = [v_{ds-PMSG} \; v_{qs-PMSG} \; \lambda_m]^T \qquad (24)$$
$$Y = [i_{d-PMSG} \; i_{q-PMSG} \; \omega_e]^T \qquad (25)$$

For the power grid model, the X, U, and Y are written as follows:

$$X = [i_{d-Grid} \; i_{q-Grid}]^T \qquad (26)$$
$$U = [v_{ds-Grid} \; v_{qs-Grid}]^T \qquad (27)$$
$$Y = [i_{d-Grid} \; i_{q-Grid}]^T \qquad (28)$$

where $v_{ds-Grid}$ and $v_{qs-Grid}$ denote dq-axes network voltages.

In this investigation, the error signal between the set-point and actual signals denote the performance index J. The error signal is the input to the LQR controller. In an instant, for LQR-1 presented in Fig. 5, the reference and measured signals are ω_r^* and $\widehat{\omega}_r$ respectively, and the output of LQR controller represents the torque command (T_e^*).

The optimal values of Q and R used in this investigation are chosen to reach the optimal performance along with an economical cost as follows:

$Q = [Q\text{-}1 \; Q\text{-}2] = [1.18 \; 10]$; $R = [R\text{-}1 \; R\text{-}2] = [0.7 \; 2]$.

In this study, the MATLAB command "$[K] =$ LQR (A, B, Q, R)" is used to obtain the optimal gain K, where the values of A and B are determined from the linearized system. The values of K for the system under study are determined as follows:

$K = [K\text{-}1 \; K\text{-}2] = [1.2984 \; 2.2361]$.

Optimized PI controller by GWO algorithm
GWO is a novel population-based approach presented in 2014 [14]. The GWO algorithm describes the hunting behavior of the grey wolves. Grey wolves used to live in groups. The size of each group usually consists of 5-12 wolves. This group, in general, classified into four prevalent dominant types, named alpha (α), beta (β), delta (δ), and omega (ω) wolves. The α wolves represent the leader wolves in the group. They are responsible for taking social and activity works such as hunt, sleep place, and time to wake. Besides, the α wolves pursue other wolves in the group for some kind of democracy. The β wolves are the next level in the pack, who help and support α wolves in decisions-making. The β wolf is the best candidate to α wolf when α wolf dies or becomes too old. The β wolves are responsible for helping the α wolves and reinforce their order in the group. The final level of dominance in the group is the ω wolves, which are the last wolves that are allowed to eat. Sometimes, the ω wolves are the babysitters in the group. The δ wolves take the responsibility for presenting sufficient knowledge to α and β wolves; however they dominate ω wolves. The steps of hunting process of the grey wolves are broadly categorized as [16]–[18]:
1. Tracking, chasing, and approaching the prey.
2. Encircle and harass the prey until it stops moving.
3. Attack to the prey.
In this study, the GWO algorithm is used to design the values of the PI controllers, as mentioned in [3].

VII. SIMULATION RESULTS
The simulation studies are executed through the MATLAB/Simulink environment. The time step is considered 20 µs. The efficiency of the LQR controller is examined by

comparing the analyses with that realized when the GWO-based optimal PI controllers is used, considering the normal and transient operating conditions, which are discussed as follows.

A. Normal Operating Condition

The dynamic response of the VSWT driven PMSG is verified through practical wind speed data captured from Zaafarana wind farm, Egypt, as pointed out in Fig. 7(a). The simulation time is 500 s, which indicates a wide speed range of the wind speed from 8.1 to 11.8 m/s that considered in this study. Fig. 7(b) shows the responses of the measured and estimated generator speeds. It can be noted here that the measured PMSG speed can track the estimated speed very well. Fig. 7(c) points out the responses of the measured and estimated rotor positions of the PMSG. Notably, the SMO technique can accurately estimate the rotor position/speed of the PMSG during all operating conditions. The optimum and grid active powers are shown in Fig. 7(d). Note that those powers are very close due to the power losses of converters. Fig. 7(e) indicates the reactive power at the GSI using the LQR controller. The terminal grid voltage at the PCC is shown in Fig. 7(f). The terminal grid current at the PCC is illustrated in Fig. 7(g). Notably, the FSTP frequency converter works very well with the VSWT-PMSG system. Moreover, the LQR controller can precisely capture the maximum power from the wind and deliver it to the utility grid during different operating conditions.

TABLE I
PMSG EXPERIMENTAL SETUP PARAMETERS.

Parameters	Values
Nominal voltage	117 V rms (ph-to-n)
System frequency	50 Hz
Dc-link voltage	350 V
Dc-link capacitance	350 µF
Filter inductance	3.3 mH
Grid inductance	0.8 mH
PMSG rated power	5 kW
Number of poles	22
PMSG rated speed	240 rpm
PMSG winding resistance	0.84 Ω
PMSG winding d-axis inductance	12.6 mH
PMSG winding q-axis inductance	21.8 mH

TABLE II
CONTROLLER GAINS USING GWO

Controllers Gains	Notation	GWO
Vdc outer-loop proportional gain	Kp_{Vdc}	0.07
Vdc outer-loop integral gain	Ki_{Vdc}	1.2
Vpcc outer-loop proportional gain	Kp_{Vpcc}	0.3
Vpcc outer-loop integral gain	Ki_{Vpcc}	1.5
Inner - loop proportional gain	Kp_{GSC}	5
Inner - loop integral gain	Ki_{GSC}	26

VIII. CONCLUSION

This thesis has proposed an LQR control scheme to optimally control the FSTP frequency converter with a view to improve the characteristics of the WECS. The proposed control scheme was introduced to control the MSC and the GSI. The rotor position and speed of the PMSG have been estimated using the SMO algorithm. Therefore, eliminating the rotor position/speed sensors with reducing the number of utilizing power switches will be advantageous in terms of cost/losses, and reliability. The simulation and experimental results have proven the validation of the LQR controller in obtaining the best responses by comparing the results to that realized when the GWO algorithm-based optimized PI control strategy is employed. The transient specifications like maximum percentage overshoot, undershoot, rise time, settling time, and steady state error of several quantities are smaller using the LQR controller and these specifications with the LQR controller are lower than that achieved by the PI controller by at least 20%. Moreover, the LQR controller is very simple, easy to implement, and has a lower memory capacity. The results have also shown its verification of smooth dynamic operation under real wind speed data extracted from a wind power plant. It can be concluded that the LQR is an optimal control approach that has the capability to deal well with the system uncertainty and enhancing system stability.

REFERENCES

[1] Global Wind Energy Council (GWEC), "Annual market update 2015," Global Wind Report, available at: http://www.gwec.net

[2] X. Zeng, J. Yao, Z. Chen, W. Hu, Z. Chen, and T. Zhou, "Co-ordinated control strategy for hybrid wind farms with PMSG and FSIG under unbalanced grid voltage condition," IEEE Trans. Sustain. Energy, vol. 7, no. 3, pp. 1100–1110, 2016.

[3] Mahmoud A. Soliman, Hany M. Hasanien, Haitham Z. Azazi, et al., "Hybrid ANFIS-GA-based control scheme for performance enhancement of a grid-connected wind generator," IET Renew. Power Gener., vol. 12, no. 7, pp. 832–843, 2018.

[4] Z. Zhang, F. Wang, J. Wang, J. Rodríguez, and R. Kennel, "Nonlinear direct control for three-level NPC back-to-back converter PMSG wind turbine systems: experimental assessment with FPGA," IEEE Trans. Ind. Inf., vol. 13, no. 3, pp. 1172–1183, 2017.

[5] J. Chen, T. Lin, C. Wen, and Y. Song, "Design of a unified power controller for variable-speed fixed-pitch wind energy conversion system," IEEE Trans. Ind. Electron., vol. 63, no. 8, pp. 4899–4908, 2016.

[6] Mahmoud A. Soliman, Hany M. Hasanien, Haitham Z. Azazi, et al., "An adaptive fuzzy logic control strategy for performance enhancement of a grid-connected PMSG-based wind turbine," IEEE Trans. Ind. Inf., vol. 15, no. 6, pp. 3163-3173, June 2019.

[7] M. K. Metwally and H. Z. Azazi, "Four-switch three-phase inverter performance fed sensorless speed control induction motor drives using model reference adaptive system," Elect. Power Compon. Syst., vol. 42, no. 7, pp. 727–736, 2014.

[8] D. Zhou, J. Zhao, and Y. Liu, "Predictive torque control scheme for three-phase four-switch inverter-fed induction motor drives with DC-link voltages offset suppression," IEEE Trans. Power Electron., vol. 30, no. 6, pp. 3309–3318, 2015.

[9] Hany M. Hasanien and S. M. Muyeen, "Particle swarm optimization-based superconducting magnetic energy storage for low-voltage ride-through capability enhancement in wind energy conversion system," Elect. Power Compon. Syst., vol. 43, no. 11, pp. 1278–1288, 2015.

[10] Hany M. Hasanien, "Shuffled frog leaping algorithm-based static synchronous compensator for transient stability improvement of a grid-connected wind farm," IET Renew. Power Gener., vol. 8, no. 6, pp. 722–730, 2014.

[11] M. N. Ambia, H. M. Hasanien, A. Al-Durra, and S. M. Muyeen, "Harmony search algorithm-based controller parameters optimization for a distributed-generation system," IEEE Trans. Power Del., vol. 30, no. 1, pp. 246–255, Feb. 2015.

[12] Hany M. Hasanien, "Design optimization of PID controller in automatic voltage regulator system using Taguchi combined genetic algorithm method," IEEE Syst. J., vol. 7, no. 4, pp. 825–831, 2013.